

Lamprophyre Rocks in the Nassara Gold Deposit, Southwest Burkina Faso: Characteristics and Implication for Mining Exploration

Pascal Ouiya^{1,2*}, Adama Ouédraogo Yaméogo^{2,3}, Sâga Sawadogo², Séta Naba²

¹Ecole Normale Supérieure (ENS), Institut Sciences et Technologie (IST), Ouagadougou, Burkina Faso

²Laboratoire Géosciences et Environnement (LaGE), Earth Sciences Department, Ouagadougou, Burkina Faso

³University Norbert ZONGO (UNZ), Koudougou, Burkina Faso

Email: *pascal.ouiya@gmail.com

How to cite this paper: Ouiya, P., Yaméogo, A.O., Sawadogo, S. and Naba, S. (2023) Lamprophyre Rocks in the Nassara Gold Deposit, Southwest Burkina Faso: Characteristics and Implication for Mining Exploration. *Open Journal of Geology*, **13**, 1291-1311.
<https://doi.org/10.4236/oig.2023.1312056>

Received: October 26, 2023

Accepted: December 10, 2023

Published: December 13, 2023

Copyright © 2023 by author(s) and Scientific Research Publishing Inc. This work is licensed under the Creative Commons Attribution International License (CC BY 4.0).
<http://creativecommons.org/licenses/by/4.0/>



Open Access

Abstract

The lamprophyres are late dykes that cut the formations hosting the gold mineralization in the Nassara deposit. They are geographically and spatially related to most orogenic gold deposits. It is with the aim of characterizing them and seeing their implications for exploration that this work is carried out. To achieve our objective, petrographic studies and chemical analyses of minerals (pyroxenes, amphiboles, feldspars, chromite) and geochemical analyses of total rock were carried out. These studies have enabled us to classify the Nassara lamprophyres as calc-alkaline lamprophyres of the spessartite type. The Cr, Co, Ni and Mg enrichment of these rocks would indicate a depleted mantle source, with LILE enrichment by fluids probably related to metasomatic activity. The various diagrams show that they are depleted in HREE and enriched in LREE. The high Nb/Ta ratios in our data indicate metasomatic activity probably linked to amphibole and rutile in the mantle prior to melting. The geodynamic context of spessartite-type lamprophyres indicates a signature linked to late-orogenic to post-collisional subduction. They are late-orogenic to post-collisional lamprophyres enriched in compatible elements (Cr, Ni, Co) and display a negative Ta-Nb-Ti (TNT) anomaly. The frequent association of these lamprophyre dykes with the deposits does not indicate the source of the gold for these deposits, but rather zones of crustal permeability capable of draining hydrothermal fluids at the time of emplacement. Good mapping of lamprophyre dykes, especially in shear zones, could therefore guide prospecting and identify potential zones of hydrothermal fluid circulation.

Keywords

Nassara, Calc-Alkaline Lamprophyre, Metasomatic Activity, LILE, HREE, LREE

1. Introduction

Lamprophyres are mesocratic to melanocratic magmatic rocks that are very often associated with orogenic or non-orogenic gold deposits. They generally exhibit simple textural relationships with particulate mineralogical and chemical compositions. In the field, these rocks appear as dykes and rarely as lava flows. They are rocks formed from a small volume of biotite and/or amphibole phenocrystalline magma, with clinopyroxenes in a feldspar matrix background. For the same SiO₂ content, these rocks have relatively higher concentrations of P₂O₅, S, CO₂, K, Na, H₂O, Rb and Ba than other magmatic rocks.

Previous work ([1] [2] [3]) has highlighted five possible magmatic sources for lamprophyres: 1) calc-alkaline lamprophyres (CAL), 2) alkaline lamprophyres (AL), 3) ultramafic lamprophyres (UML), 4) lamproite lamprophyres (LL) and 5) kimberlitic lamprophyres (LK). Calc-alkaline lamprophyres, or K-rich andesites, are mafic and rich in compatible elements such as Cr, Co and Ni, with a high Ni/MgO ratio. Their minerals are similar to those of basalts, but they are richer in LILE and LREE ([4] [5] [6]). Calc-alkaline lamprophyres are generally found in lithospheric convergence environments, while alkaline and ultramafic types are associated with divergence environments or zones. Kimberlitic lamprophyres, on the other hand, are characteristic of intra-plate zones ([7]).

The aim of this paper is to constrain the nature, source and petrogenesis of the lamprophyres in order to establish their possible link to the Nassara orogenic gold deposit in southwestern Burkina Faso, and thus open up new avenues for exploration. To do this, we used mineral chemistry and major and trace element geochemical data. We then compare the Nassara calc-alkaline lamprophyres with other calc-alkaline lamprophyres to establish their source and petrogenesis.

2. Geological Context of the Nassara Zone and Lamprophyres

The Paleoproterozoic formations of West Africa, known as the Birimian formations, correspond to a geological period around 2.1 Ga. They occupy around 80% of the surface area of Burkina Faso (**Figure 1**) and correspond to a period of crustal growth that took place during the Eburnian orogeny ([8]). These formations are organized in greenstone belts consisting mainly of metavolcanic and metasedimentary rocks, at the boundaries of which are large batholiths. The Nassara gold deposit is located south of Gaoua in the Boromo greenstone belt, more precisely in the Batié West shear zone ([9]). The Boromo belt consists of volcanic and volcanosedimentary rocks cut by different generations of granitoids

([9] [10] [11] [12]) show that this belt contains tholeiitic basalts, often in pillow lavas and locally containing plagioclase phenocrysts, gabbros in the western part and ultramafics in the eastern part, calc-alkaline basalts, andesites and rhyolites. Three deformation phases affect these rocks. These are phases D1, D2 and D3, characterized respectively by S1, S2 and S3 schistosities ([9] [13] [14] [15]).

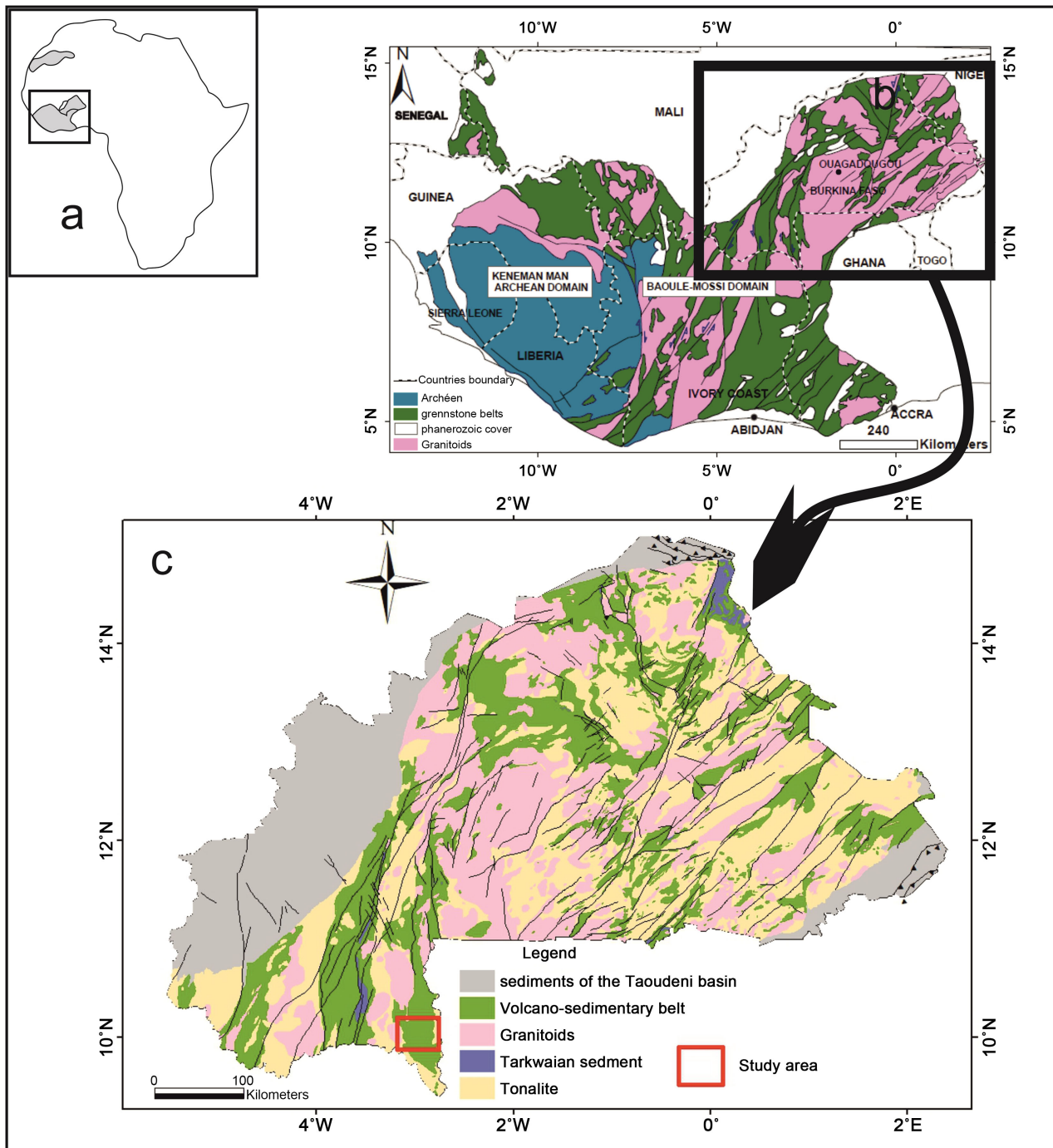


Figure 1. Regional geological setting of the study area: (a) Location of the Man/Leo Ridge in West Africa; (b) Location of Burkina Faso on the simplified geological map of the Man/Leo Ridge and (c) Location of the study area (red box) on the litho-structural map of Burkina Faso.

Volcanic rocks in the Nassara gold deposit are represented by tholeiitic basalts, basaltic andesites, andesites, dacites, rhyodacites and rhyolites. The Nassara gold deposit (**Figure 2**) ([16]) lies at the contact between volcanic rocks (basalt-andesite) and sedimentary rocks (pyroclastite and black shale). This ensemble is later cut by late diorite and lamprophyre dykes.

3. Methodology and Analytical Techniques

Samples were taken in the field from lamprophyre dykes and used to make thin sections for microscopic studies. Minerals of interest were identified during the course of this study for electron microprobe chemical analysis at the Geosciences Laboratory in Toulouse (GET). In all, over forty points of analysis were carried out on different minerals. Two lamprophyre dyke samples were analyzed for total rock chemistry using Inductively Coupled Plasma-mass spectrometry and Atomic Emission Spectrometers (ICP-MS and ICP-AES) at ALS (Spain). For more details on the procedure for this type of analysis, please consult the laboratory's website (<https://www.alsglobal.com>).

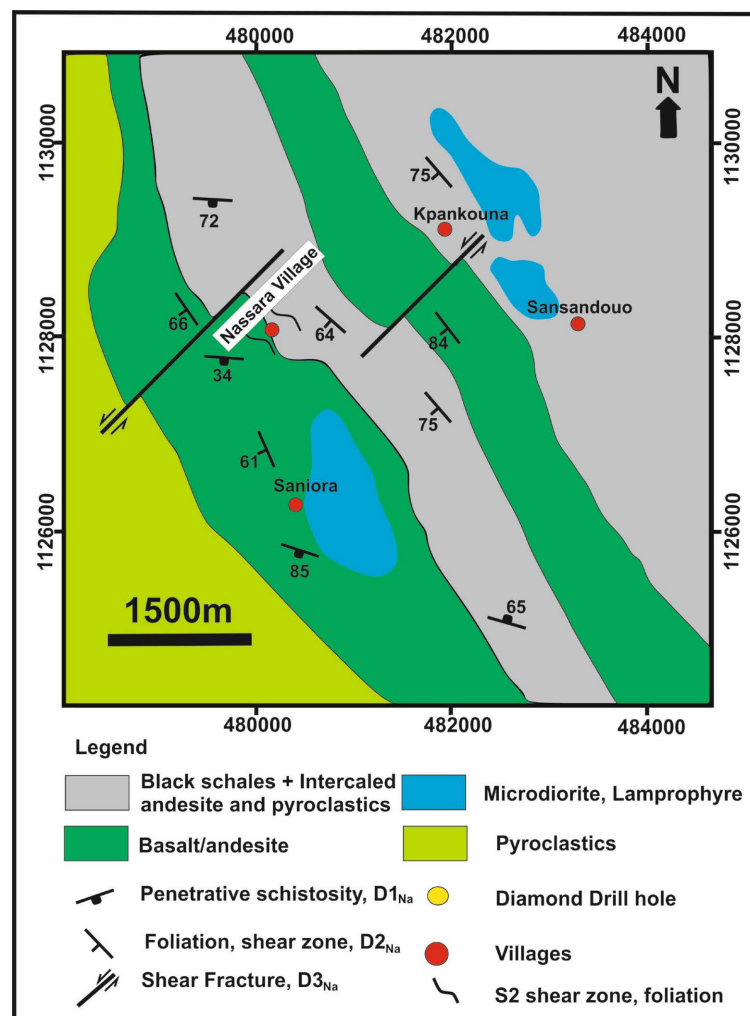


Figure 2. Litho-structural map of the study area.

4. Petrography of Lamprophyric Dykes

Lamprophyre dykes are rocks in the form of small isolated massifs that outcrop within the Nassara gold deposit (**Figure 3a**). Macroscopically, they are massive rocks with local enclaves of leucogranite (**Figure 3b**). At this scale, phenocrysts of amphibole and pyroxene can be seen in a whitish background of mainly feldspar. All these primary minerals are more or less well preserved. Microscopic observations show that the rock is composed mainly of potassic feldspars, albite, pyroxenes and amphibole (**Figures 4a-d**).

These minerals are locally altered to form secondary minerals. Clinopyroxenes (Cpx), for example, alter to give tremolites and chlorites (**Figure 4a**, **Figure 4c**). Amphiboles alter into chlorites and chromites (**Figure 4d**, **Figure 4e**). When alteration is much more advanced, amphiboles can give chlorites and muscovites (**Figure 4e**), while pyroxenes give tremolites, rutiles and chlorites (**Figure 4e**, **Figure 4f**).

5. Mineralogy

Some forty analysis points were analyzed by electron microprobe at the Laboratoire Géosciences Environnement Toulouse. Representative mineral compositions of pyroxenes, hornblende, chromites and feldspars from the lamprophyre dyke are shown in **Tables 1-4**.

5.1. Pyroxenes

Pyroxene analysis data (**Table 1**) have been plotted in four diagrams (**Figure 5** and **Figure 6**). In the binary diagram (Al_2O_3 - Cr_2O_3), the data reveal a clinopyroxene composition (**Figure 5a**). And more precisely, augite to a lesser extent diopside in the ternary Wo-En-Fs diagram (**Figure 5b**). Augites are located in the field of tholeiitic basalts and calc-alkaline basalts in the binary diagram (Ti vs. Na + Ca) of ([17]) (**Figure 6a**). Clinopyroxenes from Nassara lamprophyres are more enriched in Al_2O_3 and Cr_2O_3 than clinopyroxenes from gabbros ([18]). The Ti vs. Al IV binary diagram confirms that these are augites from tholeiitic and calc-alkaline basalts (**Figure 6b**).

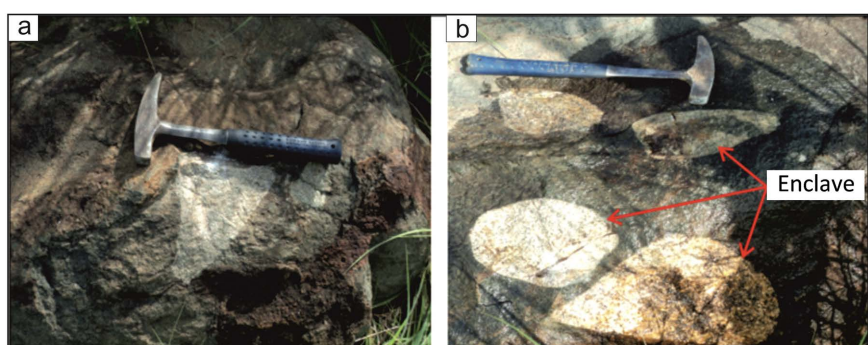


Figure 3. Field images of the lamprophyre dyke: (a) Patina color (grayish) covered by a thin layer of iron oxide (reddish), (b) Lamprophyre dyke with leucogranite enclaves.

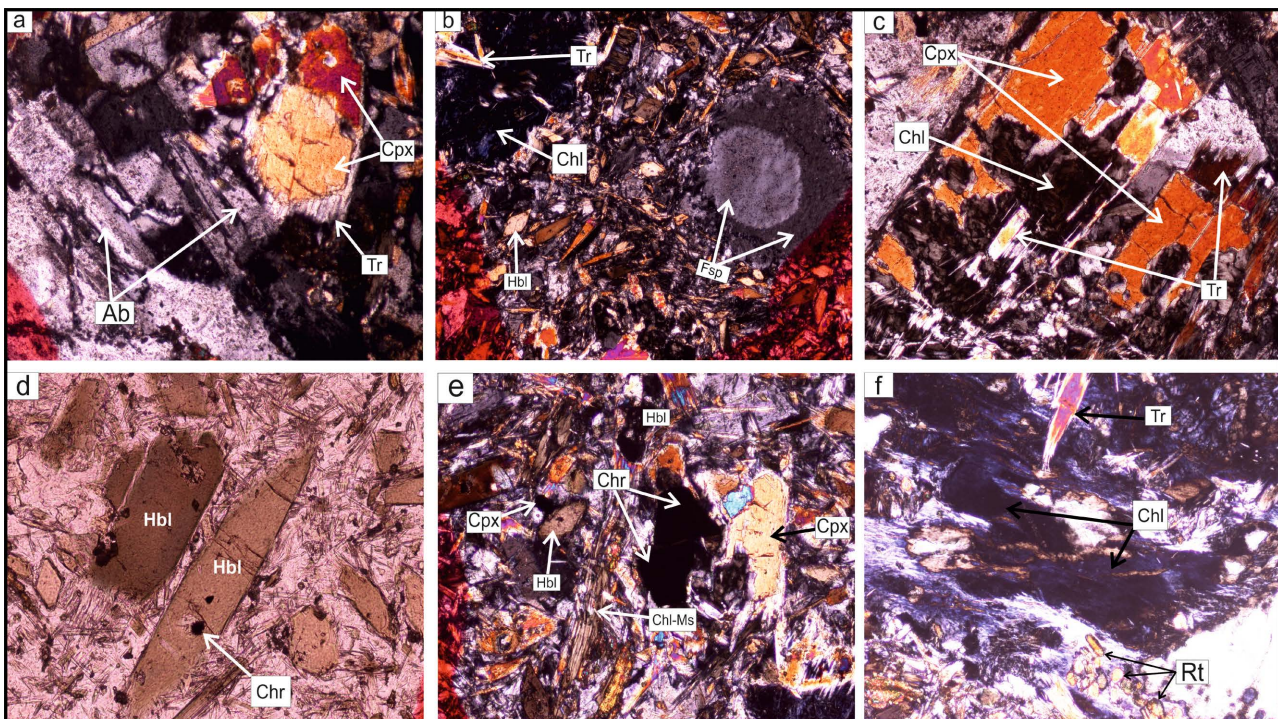


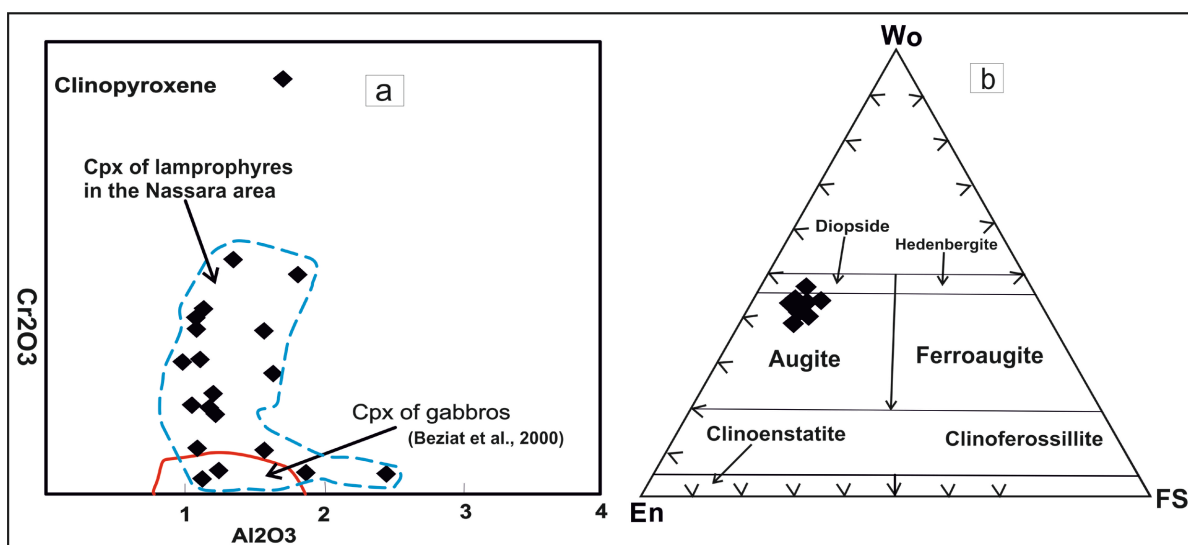
Figure 4. Microphotographs of the lamprophyres: (a) beach showing albite crystals and clinopyroxene crystals locally altered to tremolite, (b) Range showing tremolite and chlorite in a potassic feldspar background, (c) Clinopyroxene megacrystal (Cpx) locally altered to chlorite (Chl) and tremolite (Tr), (d) Image showing hornblende crystals (Hbl) in a microcrystalline feldspar matrix, (e) Image showing Hbl altered to Chl and muscovite (Ms). Clinopyroxenes are destabilized to chromites (Chr), (f) Destabilization of lamprophyre primary minerals to tremolite (Tr), chlorite and rutile crystals (Rt).

Table 1. Representative microprobe analysis of pyroxenes.

	PX1	PX2	PX3	PX4	PX5	PX6	PX7	PX8	PX9	PX10	PX11	PX12	PX13	PX14	PX15	PX16
SiO ₂	53.56	54.29	53.36	53.12	52.89	53.30	53.54	53.57	52.66	53.05	52.57	53.29	53.60	53.01	53.65	51.88
TiO ₂	0.22	0.156	0.202	0.262	0.246	0.198	0.189	0.218	0.311	0.202	0.301	0.26	0.241	0.125	0.164	0.34
Al ₂ O ₃	1.11	1.05	1.35	1.1	1.18	1.13	0.98	1.12	1.63	1.70	1.81	1.21	1.21	1.88	1.08	2.47
Cr ₂ O ₃	0.44	0.29	0.77	0.14	0.28	0.62	0.43	0.04	0.39	1.37	0.72	0.26	0.33	0.07	0.58	0.06
FeO	5.49	6.63	4.85	7.32	6.42	4.79	5.15	7.51	7.19	4.64	5.48	6.28	6.15	7.85	4.77	7.99
MnO	0.18	0.23	0.14	0.21	0.16	0.15	0.15	0.25	0.25	0.19	0.07	0.21	0.22	0.21	0.12	0.24
MgO	17.17	17.73	17.10	16.49	16.27	16.81	17.33	16.23	16.29	17.04	16.26	16.66	16.46	15.98	17.29	14.38
CaO	21.11	19.83	21.79	20.31	20.81	21.74	21.11	20.61	20.55	20.86	21.54	21.22	21.39	20.16	22.07	20.87
Na ₂ O	0.28	0.24	0.31	0.19	0.32	0.26	0.22	0.27	0.31	0.45	0.39	0.31	0.32	0.43	0.29	0.53
K ₂ O	0	0.01	0	0	0	0.004	0.012	0.01	0	0	0.02	0.01	0.01	0.01	0.01	0
Total	99.56	100.45	99.8	99.14	98.58	98.99	99.12	99.82	99.58	99.5	99.18	99.7	99.9	99.72	100.02	98.77
Ca	0.83	0.77	0.86	0.81	0.83	0.86	0.83	0.82	0.82	0.82	0.85	0.84	0.84	0.8	0.86	0.84
Na	0.02	0.02	0.02	0.01	0.02	0.02	0.015	0.019	0.022	0.032	0.028	0.022	0.023	0.03	0.021	0.038
Na + Ca	0.85	0.79	0.87	0.82	0.85	0.88	0.85	0.83	0.84	0.85	0.88	0.86	0.86	0.83	0.88	0.87
En	48.34	49.47	48.1	46.68	46.59	47.76	48.84	45.85	46.24	49.05	46.65	46.87	46.48	45.67	48.17	42.29
Fs	8.96	10.75	7.86	11.97	10.58	7.87	8.39	12.30	11.85	7.79	8.93	10.23	10.09	12.92	7.65	13.59
Wo	42.71	39.78	44.04	41.34	42.83	44.37	42.77	41.85	41.91	43.15	44.41	42.89	43.42	41.40	44.17	44.12

Table 2. Representative microphobe analyses of amphiboles and tremolites.

	Amphiboles							Tremolite	
	1	2	3	4	5	6	7	1	2
SiO ₂	42.67	40.33	41.49	40.65	42.47	54.38	50.75	56.55	56.48
TiO ₂	1.82	1.95	1.91	1.84	1.61	0.04	0.16	0.01	-
Al ₂ O ₃	11.41	10.55	12.21	12.62	11.57	1.42	3.49	0.29	0.67
FeO	11.95	12.51	13.34	14.18	13.62	13.27	15.23	8.42	8.03
MnO	0.19	0.24	0.23	0.22	0.18	0.52	1.01	0.13	0.14
MgO	13.39	11.86	12.73	11.53	12.53	14.74	12.83	18.50	18.55
CaO	11.73	13.71	11.66	11.67	11.49	12.35	11.90	13.05	13.28
Na ₂ O	2.13	2.05	2.10	2.16	2.11	0.39	0.73	0.11	0.11
K ₂ O	0.98	0.75	1.02	1.11	0.66	0.07	0.26	0.06	0.04
Cr ₂ O ₃	0.004	0.01	-	0.03	-	0.08	0.02	-	0.45
Total	97.25	94.73	96.93	96.29	96.32	97.33	96.41	97.15	97.85
Si	6.33	6.28	6.15	6.13	6.31	7.88	7.52	8.00	7.93
Cr	-	-	-	-	-	0.01	-	-	0.05
Fe ³⁺	0.40	-	0.62	0.45	0.60	0.02	0.27	-	-
Fe ²⁺	1.07	1.62	1.02	1.33	1.08	1.58	1.61	0.99	0.94
Mn	0.02	0.03	0.03	0.03	0.02	0.06	0.12	0.01	0.01
Mg	2.96	2.75	2.81	2.59	2.77	3.18	2.83	3.90	3.88
Ca	1.86	2.28	1.85	1.88	1.82	1.91	1.88	1.97	2.00
Na	0.61	0.61	0.60	0.63	0.61	0.11	0.21	0.03	0.03
K	0.18	0.15	0.19	0.21	0.13	0.01	0.05	0.01	0.01
(Ca + Na) (B)	2	2.28	2	2	2	2	2	2	2.00
Na (B)	0.13	-	0.14	0.11	0.17	0.08	0.11	0.02	-
(Na + K) (A)	0.66	0.76	0.65	0.73	0.56	0.04	0.15	0.02	0.03
Mg/(Mg + Fe ²)	0.73	0.63	0.73	0.67	0.71	0.66	0.64	0.79	0.80

**Figure 5.** Composition of lamprophyre pyroxenes. (a) Composition field in the binary diagram (Al₂O₃-Cr₂O₃), (b) Composition field in the ternary diagram (Wo-En-Fs).

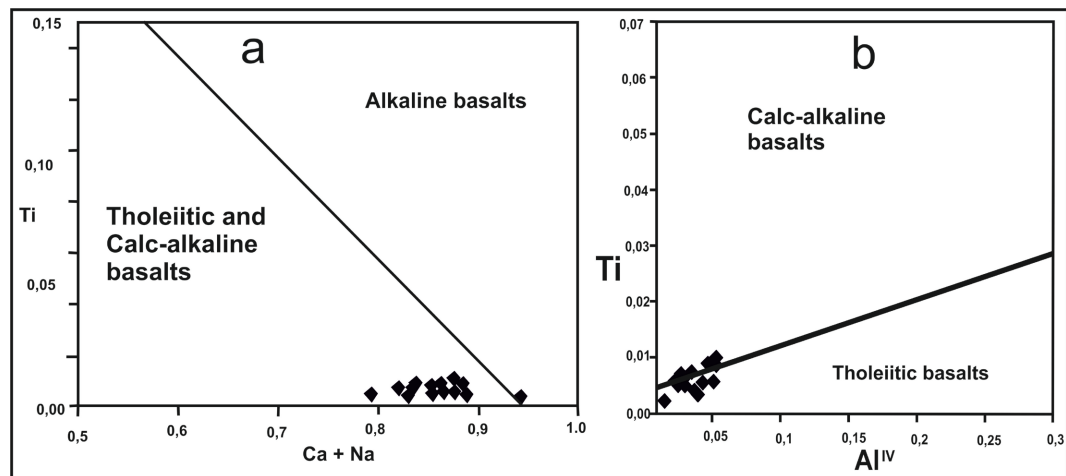


Figure 6. Geodynamic framework of pyroxenes in lamprophyres. (a) Binary diagram ($\text{Na} + \text{Ca}$) vs Ti showing pyroxenes from tholeiitic to calc-alkaline basalts, (b) Binary diagram Ti vs Al^{IV} showing the same trends for tholeiitic to calc-alkaline basalts ([17]).

Table 3. Representative microprobe analyses of chromes and albites.

	Chromites								Albitess		
	1	2	3	4	5	6	7	8	1	2	
SiO_2	0.036	0.09	0.07	0.11	0.04	0.13	0.18	0.12	SiO_2	68.79	68.69
Al_2O_3	6.81	7.54	7.05	5.72	10.17	5.94	6.09	6.02	Al_2O_3	19.57	19.82
FeO	24.89	24.98	20.99	18.53	25.12	20.50	22.15	21.9	Fe_2O_3	0.059	0.05
MnO	-	-	-	-	-	0.33	0.35	0.34	CaO	0.058	0.20
MgO	7.622	8.05	10.19	11.24	10.57	9.86	8.61	9.21	Na_2O	12.08	12.07
TiO_2	0.309	0.31	0.32	0.24	0.78	0.31	0.19	0.24	K_2O	0.07	0.06
Cr_2O_3	58.374	57.60	59.56	61.54	51.0	60.78	59.84	60.21	Total	100	100
NiO	0.12	0.14	0.12	0.17	0.15	-	-	-	Si	2.98	2.98
Total	98.16	98.72	98.32	97.55	97.85	97.86	97.44	98.06	Al^{IV}	1.003	1.01
Si	0.001	0.003	0.002	0.003	0.001	0.004	0.006	0.004	Fe^{3+}	0.002	0.002
Al	0.27	0.30	0.28	0.23	0.39	0.24	0.25	0.24	Ca	0.003	0.01
Fe^{3+}	0.12	0.13	0.11	0.11	0.23	0.10	0.10	0.11	Na	1.02	1.015
Fe^{2+}	0.60	0.58	0.47	0.42	0.46	0.48	0.54	0.51	K	0.004	0.004
Mn	-	-	-	-	-	0.01	0.01	0.01			
Mg	0.39	0.41	0.51	0.57	0.52	0.5	0.44	0.47			
Ti	0.01	0.007	0.008	0.006	0.01	0.008	0.005	0.006			
Cr	1.59	1.55	1.59	1.65	1.34	1.64	1.64	1.63			
Ni	0.002	0.003	0.002	0.004	0.003	-	-	-			
100 $\text{Mg}/(\text{Mg} + \text{Fe})$	39.55	41.36	51.83	57.51	53.22	51.08	45.17	47.82			
100 $\text{Cr}/(\text{Cr} + \text{Al})$	85.17	83.66	84.99	87.83	77.08	87.28	86.8	87.01			
Cr/M^{3+}	0.79	0.77	0.79	0.82	0.67	0.82	0.82	0.81			
Al/M^{3+}	0.13	0.15	0.14	0.11	0.19	0.11	0.12	0.12			
$\text{Fe}^{3+}/\text{M}^{3+}$	0.05	0.06	0.05	0.05	0.11	0.05	0.05	0.05			
$\text{Fe}^{2+}/\text{M}^{2+}$	0.60	0.58	0.48	0.42	0.46	0.48	0.54	0.52			
Mg/M^{2+}	0.39	0.4	0.51	0.57	0.53	0.50	0.44	0.47			
$\text{Mg}/(\text{Mg} + \text{Fe}^{2+})$	0.99	0.99	0.99	0.99	0.98	0.98	0.98	0.98			
$\text{Mg}/(\text{Mg} + \text{Fe}^{3+})$	0.39	0.41	0.51	0.57	0.53	0.51	0.45	0.47			

Table 4. Representative major (wt%) and trace (ppm) element compositions for the Nassara lamprophyres.

	Nassara lamprophyres			Syama lamprophyre	
	Major elements (wt%)				
SiO ₂	53.2	51.3	39	43.3	37.7
Al ₂ O ₃	11.4	11.2	6.6	8.9	13.4
Fe ₂ O ₃	8.92	8.52	8.2	9.4	16.9
CaO	7.55	7.65	9.82	7.14	6.6
MgO	11.2	10.2	10.5	9.24	9.79
Na ₂ O	2.88	2.68	0.61	1.12	1.16
K ₂ O	1.74	1.94	1.5	1.74	0.11
Cr ₂ O ₃	0.22	0.25			
TiO ₂	0.73	0.76	0.39	0.57	0.96
MnO	0.16	0.13	0.2	0.19	0.16
P ₂ O ₅	0.39	0.4	0.12	0.17	0.25
SrO	0.04	0.03	-	-	-
BaO	0.05	0.04	-	-	-
LOI	3.17	3.15	21.8	19.7	14.7
total	101.65	98.25	98.74	101.47	101.73
	Traces elements (ppm)				
Ba	498	502	243	350	51
Ce	50.3	50.1	19.1	26.5	29.3
Cr	1770	1784	1760	1140	940
Cs	0.16	0.12			
Dy	3.5	3.3	1.68	2.41	4.19
Er	1.86	1.82	0.97	1.38	2.31
Eu	1.49	1.51	0.61	0.88	1.25
Ga	16.1	16.4	-	-	-
Gd	4.34	4.04	1.82	2.78	4.37
Hf	3.1	3.23	1.4	2	3.6
Ho	0.61	0.59	0.32	0.47	0.84
La	23	26	8.3	12.4	11.7
Lu	0.25	0.3	-	-	-
Nb	5.2	5.8	2.1	3.9	5.8
Nd	26.4	25.4	10.6	14.9	19.6
Pr	6.38	6.58	2.5	3.5	4.3
Rb	18.5	17.2	48.6	59.1	3.5
Sm	5.63	5.43	2.39	3.37	5.05
Sn	1	1.02	-	-	-
Sr	354	361	371	262	107

Continued

Ta	0.3	0.32			
Tb	0.6	0.54	0.3	0.42	0.67
Th	2.67	2.35	1.1	2.13	2.51
Tl	0.5	0.6	-	-	-
Tm	0.27	0.32	-	-	-
U	1.03	1.09	-	-	-
V	176	179	125	174	306
W	3	3.02	-	-	-
Y	17.6	16.7	8.9	12.2	26.6
Yb	1.56	1.65	0.88	1.27	2.31
Zr	113	131	47	77	139
As	0.5	0.54	-	-	-
Bi	0.03	0.035			
Hg	0.01	0.011	-	-	-
Sb	0.08	0.06			
Se	0.3	0.25	-	-	-
Te	0.01	0.02			
Ag	0.5	0.55	-	-	-
Cd	0.5	0.45			
Co	44	46	43	44	42
Cu	74	81	53	63	115
Li	10	12	-	-	-
Mo	5	6	-	-	-
Ni	346	364	245	340	216
Pb	4	4.6	2	2	8
Sc	23	24.2	-	-	-
Zn	103	119	49	71	174
Ni/MgO	30.89	35.68	23.33	36.79	22.1
Nb/Pb	1.3	1.26	1.05	1.95	0.73
V/Cr	0.1	0.1	0.07	0.15	0.32
SiO ₂ /TiO ₂	72.87	67.5	100	75.96	39.27
MgO/FeO	1.25	1.19	1.28	0.98	0.58
Zrx ₃	339	393	141	231	417
Nbx50	260	290	105	195	290
Ce/P ₂ O ₅	128.97	125.25	159.16	155.88	117.2
Zr/Hf	36.45	40.55	33.57	38.5	38.61
Nb/Ta	17.33	18.13	-	-	-
Eu/Ti	2.98	2.52	-	-	-
Ba/Rb	26.91	29.19	-	-	-
Rb/Sr	0.05	0.05	-	-	-

5.2. Amphiboles

In the binary diagrams of ([19]) and ([20]), lamprohyre amphiboles are positioned in the field of magmatic pargasite-type amphiboles (blue) and in the field of secondary tremolite- or actinote-type amphiboles (orange) resulting from the partial destabilization of augites (**Figure 7a**). Cation values ((b) $\text{Ca} \geq 1.5$; (a) $(\text{Na} + \text{K}) \leq 0.5$) show that secondary amphiboles are precisely tremolites (**Figure 7b**), while cation values ((b) $\text{Ca} \geq 1.5$; (a) $(\text{Na} + \text{K}) \geq 0.5$) show that hornblendes are primary and pargasite-like (**Figure 7c**).

5.3. Chromites

Representative chromite compositions are given in **Table 3**. The presence of chromite aggregates in amphiboles or clinopyroxenes indicates the presence of destabilized olivine crystals in this type of rock. These spinels are thought to come from stratiform ultramafic-mafic complexes (**Figure 8**).

5.4. Feldspars

The representative values for feldspar composition (**Table 3**) derived from the analyses show that these are albite-type alkaline plagioclases. These feldspars, which occupy the matrix background of the lamprophyre dykes, are thought to have resulted from the destabilization of old labrador-type plagioclase crystals.

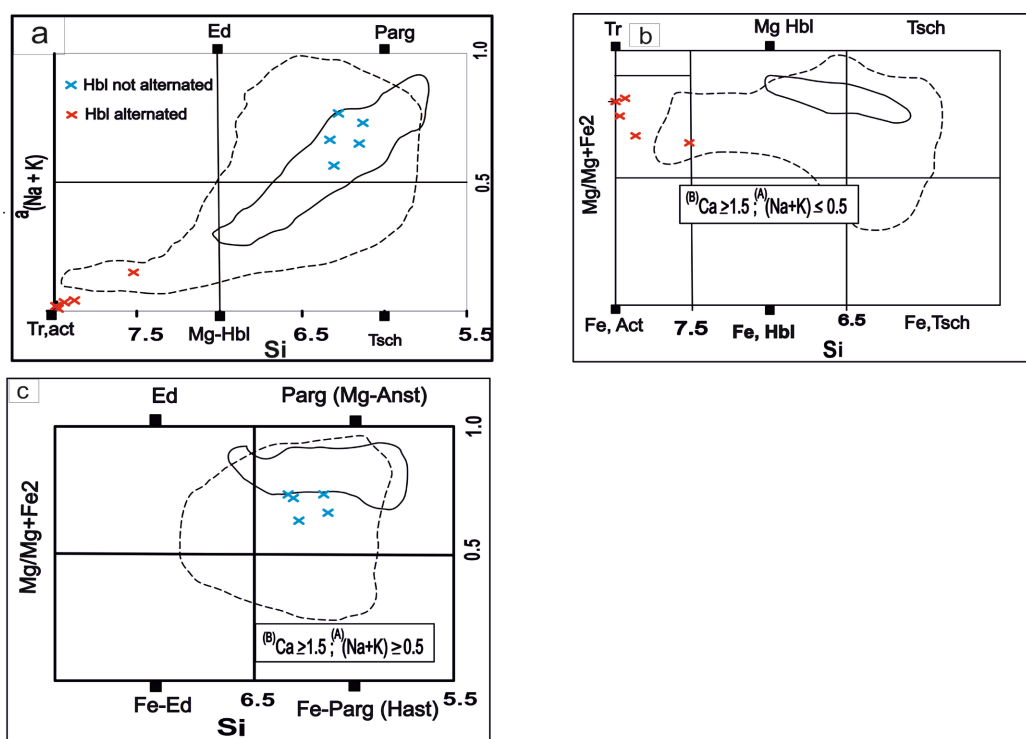


Figure 7. Champ de composition des amphiboles du lamprophyre dans les diagrammes de ([19]). (a) Diagramme binaire Si vs $a(\text{Na} + \text{K})$ montrant des amphiboles magmatiques (pargasite) et des amphiboles secondaires (trémolites et actinotes). (b) Diagramme binaire Si vs $(\text{Mg}/\text{Mg} + \text{Fe}^{2+})$ précisant la nature des amphiboles secondaires (trémolite). (c) Diagramme binaire Si vs $(\text{Mg}/\text{Mg} + \text{Fe}^{2+})$ précisant la nature des hornblendes (pargasite).

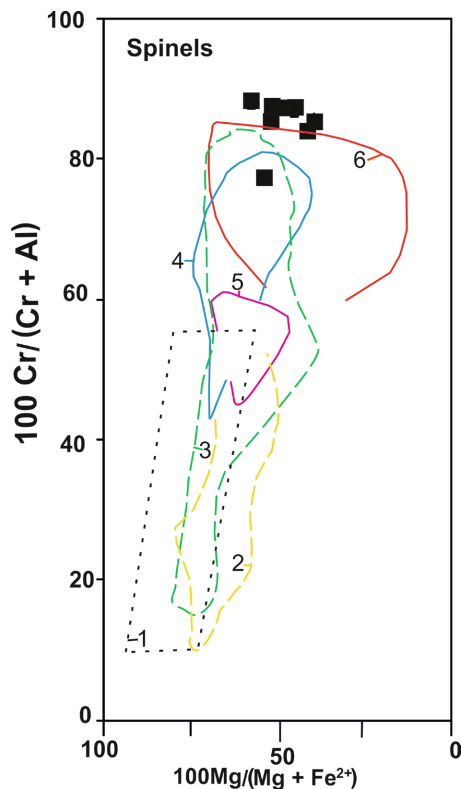


Figure 8. The spinels from which chromites are derived lie in field 6 (spinel from stratiform ultramafic-mafic complex) of the binary diagram $100 \text{ Mg}/(\text{Mg} + \text{Fe}^{2+})$ Vs $100 \text{ Cr}/(\text{Cr} + \text{Al})$. 1: Field of ophiolitic peridotite spinel from, 2: Ridge, 3: Transitional, 4: Arc (classification of [21]), 5: Field of ophiolite spinel from arc-related crust from new caledonia, ([22]) 6: Field of spinel from stratiform ultramafic-mafic complexes ([23]).

6. Geochemistry

The analytical data presented in **Table 4** show that Nassara's lamprophyric dykes contain between 51.3 - 53.2 wt% SiO_2 , between 8.52 and 8.92 wt% Fe_2O_3 , between 10.2 and 11.2 wt% MgO and 0.73 to 0.76 wt% TiO_2 . The SiO_2 vs. K_2O and Ta/Yb vs. Th/Yb diagrams from ([24]) and ([25]) respectively show that the source magma is highly potassium-rich calc-alkaline (**Figure 9**, **Figure 10**). The Nassara lamprophyres have an andesitic composition in the Nb/Y vs. Zr/TiO_2 binary diagram (**Figure 11**). The ternary $\text{MgO}-\text{Al}_2\text{O}_3-\text{K}_2\text{O}$ and binary Nb/Pb vs. V/Cr diagrams indicate lamprophyres and calc-alkaline lamprophyres respectively at Nassara (**Figure 12a**, **Figure 12b**).

In nomenclature, there are four types of calc-alkaline lamprophyre, also known as shoshonitic lamprophyre (minette, vogesite, spessartite and kersantite, e.g. ([2] [26] [27] [28])). Lamprophyre varieties are distinguished on the basis of the minerals (biotite, amphibole, orthoclase and plagioclase) that predominate in them ([29]). Based on these facts, Nassara lamprophyres are of the spessartite type, as they contain amphibole phenocrysts and labrador as feldspar.

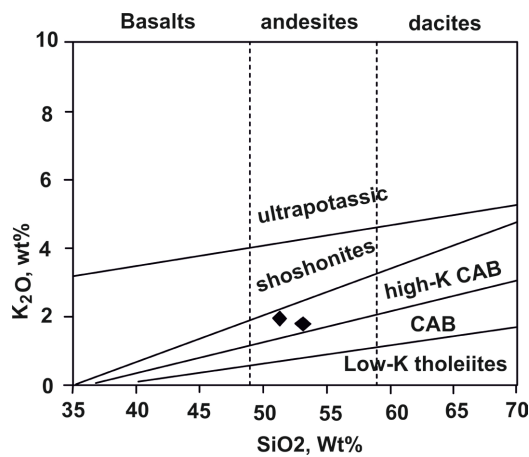


Figure 9. Nassara lamprophyres in the K_2O - SiO_2 binary diagram.

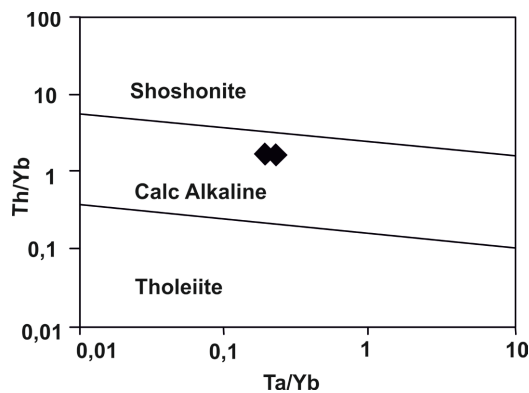


Figure 10. Nassara lamprophyres in the Th/Yb vs. Ta/Yb binary diagram.

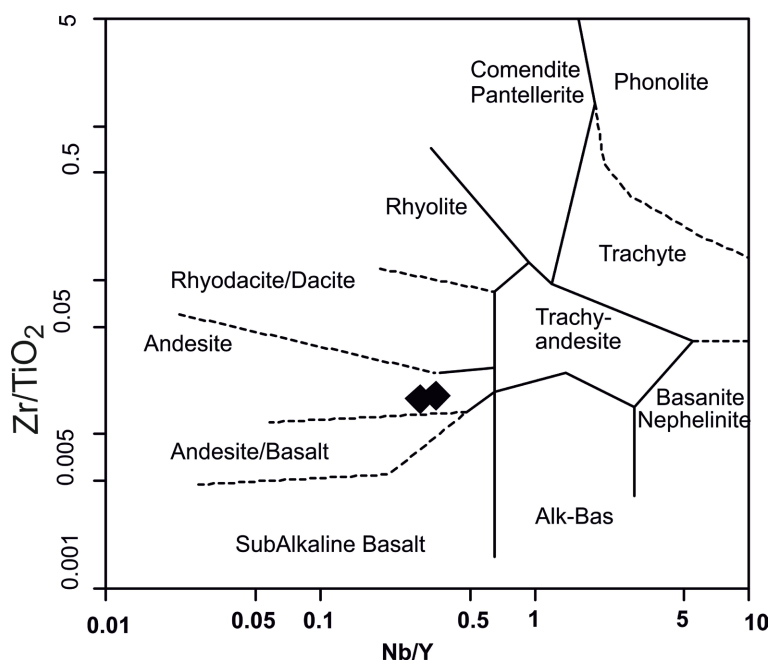


Figure 11. Nassara lamprophyres in the Zr/TiO_2 vs. Nb/Y diagram.

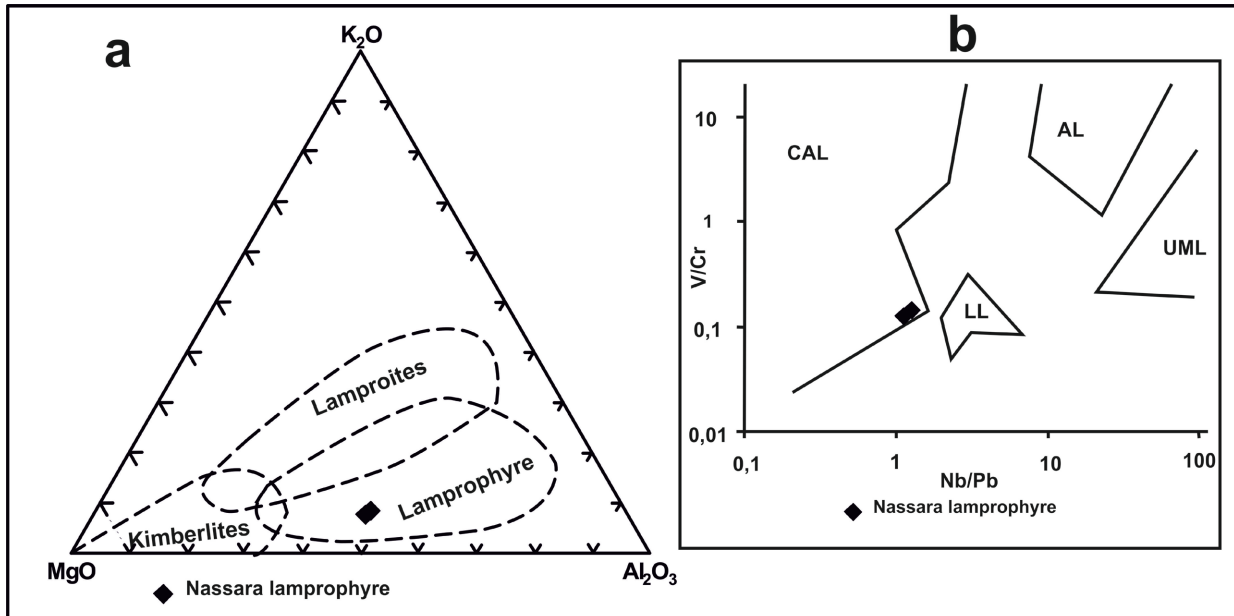


Figure 12. Lamprophyre typology diagram. (a) Positions of Nassara lamprophyres in the $\text{MgO}-\text{K}_2\text{O}-\text{Al}_2\text{O}_3$ ternary diagram, (b) Positions of Nassara lamprophyres in the V/Cr vs. Nb/Pb diagram ([2]). CAL: Calc-alkaline lamprophyres, AL: Alkaline lamprophyres, LL: Lamproite lamprophyres, ULM: Ultramafic lamprophyres.

Rare-earth spectra normalized to the primitive mantle, Nassara lamprophyres show a light rare-earth enrichment (LREE) of the order of 40 to 50 times that of chondrite, while heavy rare-earth elements (HREE) show only a weak enrichment of the order of 3 times that of chondrite (Figure 13). In comparison with lamprophyres from Syama (Mali), lamprophyres from Nassara are richer in light earth elements than those from Mali. Calc-alkaline lamprophyres are enriched in compatible elements (Cr-Ni-Co) and with negative Ta-Nb-Ti (TNT) anomalies (Figure 14). This is similar to what has been proposed ([30]) for lamprophyres from the Eslamy peninsula.

7. Discussion

All the diagrams show that these are potassium-rich calc-alkaline lamprophyres. The dominance of pargasite-type amphiboles and plagioclase proves that these are spessartite-type lamprophyres. In the nomenclature, this type of lamprophyre is dominated by hornblendes and plagioclases ([2] [27] [29]).

The enrichment in compatible elements (Cr, Co, Ni, Mg) in the spessartite-type lamprophyres at Nassara is compatible with a mantle source. Moreover, the presence of chromite aggregates in these lamprophyres proves that these rocks once contained olivine crystals. In the Al_2O_3 vs Cr_2O_3 binary diagram, these olivines are found in the mantle field, providing evidence of a mantle source for these rocks (Figure 15). As the geochemical elements Nb-Ta and Zr-Hf have similar geochemical behaviors, high ratios of Nb/Ta and Zr/Hf indicate that the source region underwent metasomatism prior to melting ([30]). These high ratios are controlled by geochemical processes such as partial melting, crystallization and

metasomatism of rutile and amphiboles in the mantle ([30] [32]). In view of the above, the high Nb/Ta ratios in the Nassara lamprophyres indicate metasomatic activity of pargasite-type amphiboles and rutiles (**Figure 4**) in the mantle prior to melting. A number of studies ([5] [30] [33]) propose a mantle-depleted source for this type of rock, with LILE enrichment by fluids linked to metasomatic activity. We propose that the Nassara lamprophyres are related to a depleted mantle with enrichment in LILE by fluids probably related to metasomatic activity in the mantle prior to its melting. This is reflected in moderate to relatively high Ce, Rb, K, Na contents in our data (**Table 4**).

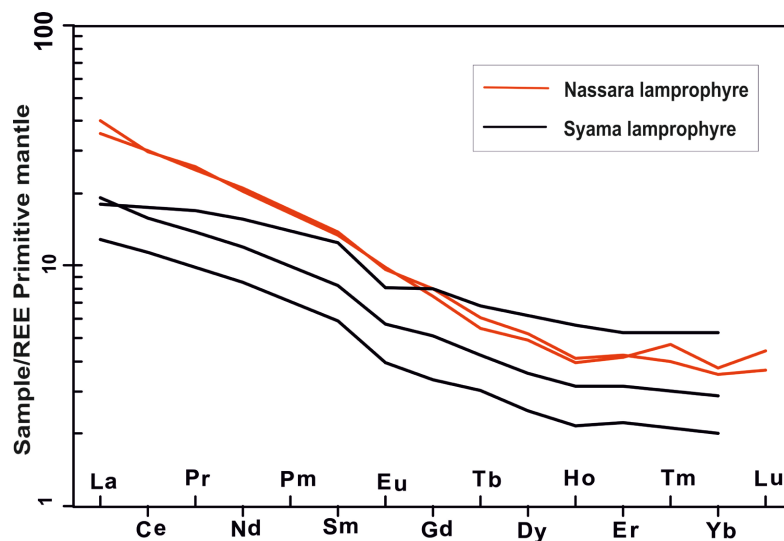


Figure 13. Diagram of rare earths normalized to the primitive mantle ([31]). Two samples for this study (Nassara area) and three in the Syama area (Mali).

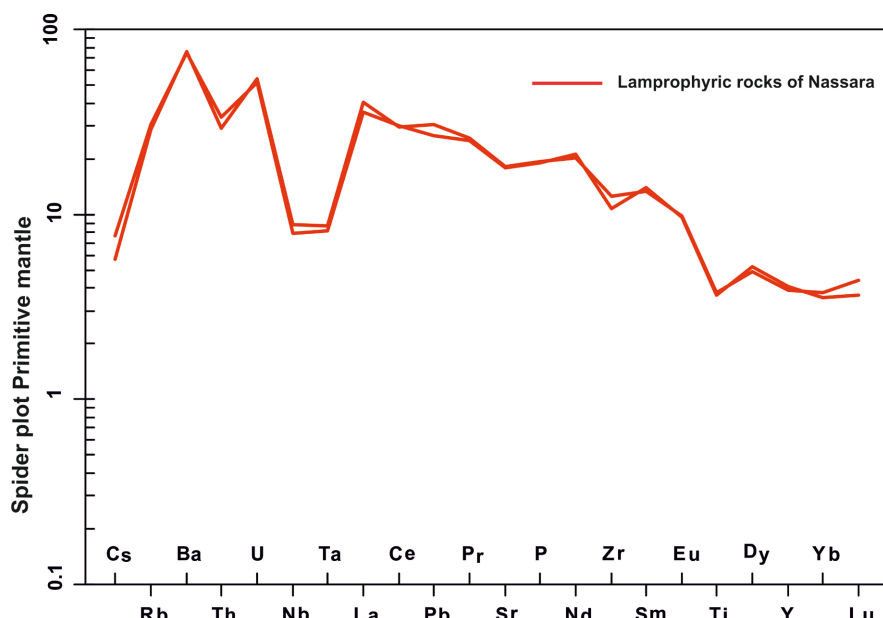


Figure 14. Multi-element diagram of the Nassara lamprophyre normalized to the primitive mantle ([31]).

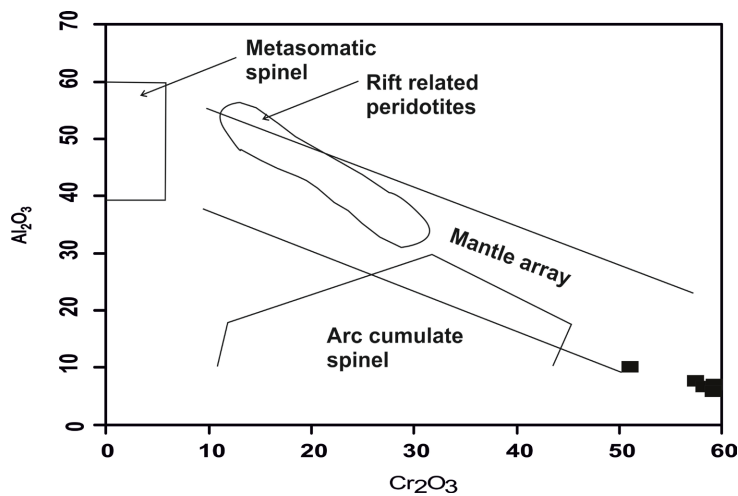


Figure 15. Field of spinels from which chromites are derived in the Al_2O_3 vs Cr_2O_3 binary diagramChamp des spinelles dont dérivent les chromites dans le diagramme binaire Al_2O_3 vs Cr_2O_3 .

To constrain the geodynamic context, our data were plotted in the ternary $\text{Ce}/\text{P}_2\text{O}_5$ -50Nb-3Zr diagram and lie within the field of post-collisional arcs (**Figure 16**). In the Th-Hf-Nb/2 ternary diagram ([34]), the Nassara lamprophyres, like those at Syama ([35]), are close to the calc-alkaline lamprophyre field, which has a geodynamic signature linked to orogenic subduction (**Figure 17a**). In the same diagram, our data and that of the lamprophyres from syama are close to the orogenic lamprophyre-lamproite-lampyrite association linked to late to post-collisional geodynamic evolution (**Figure 17b**). In view of the foregoing, the Nassara lamprophyres would appear to have a geodynamic signature related to late to post-collisional orogenic subduction for a depleted mantle source. Still based on the above, but also on **Figure 14**, the Nassara calc-alkaline lamprophyres are late-orogenic to post-collisional spessartite lamprophyres enriched in compatible elements (Cr, Ni, Co) and showing a negative Ta-Nb-Ti (TNT) anomaly.

As far as the link between gold and lamprophyres is concerned, we can see that they are spatially and closely linked to the gold deposit. Contrary to what has been proposed ([36]) that lamprophyres transported gold during their emplacement, ([37]) believe that there is no correlation between gold and LILEs, so metasomatism did not enrich the source mantle in gold. This is why some authors believe that there is no direct link between lamprophyres and gold ([38] [39] [40]). On the other hand, altered lamprophyres can be rich in gold, but this is due to the mineralizing fluid ([37] [41]).

The mineralizing fluids in the deposits follow the same structures as the lamprophyres, so they are spatially, not genetically, linked. The presence of lamprophyres in deposits is an indicator of crustal permeability capable of channeling hydrothermal fluids during emplacement. Lamprophyres can therefore be used as a prospecting guide. This leads us to say that a good mapping of lamprophyres contained in shear zones could be a good guide for prospecting.

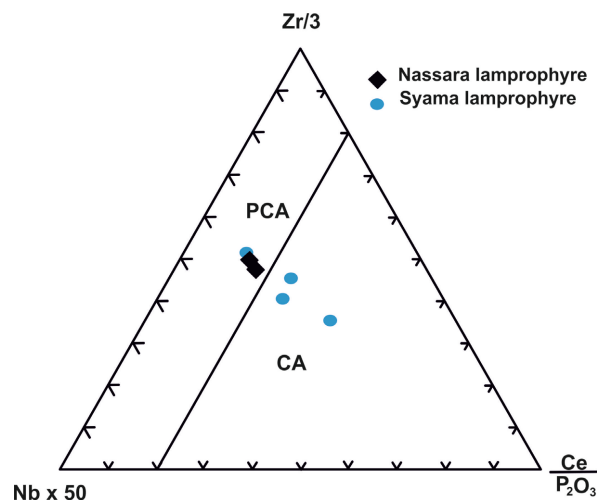


Figure 16. Positions of Nassara and Syama lamprophyres in the post-collision discrimination diagram of the geodynamic context PCA = post-collision-margin active and CA = collision margin active.

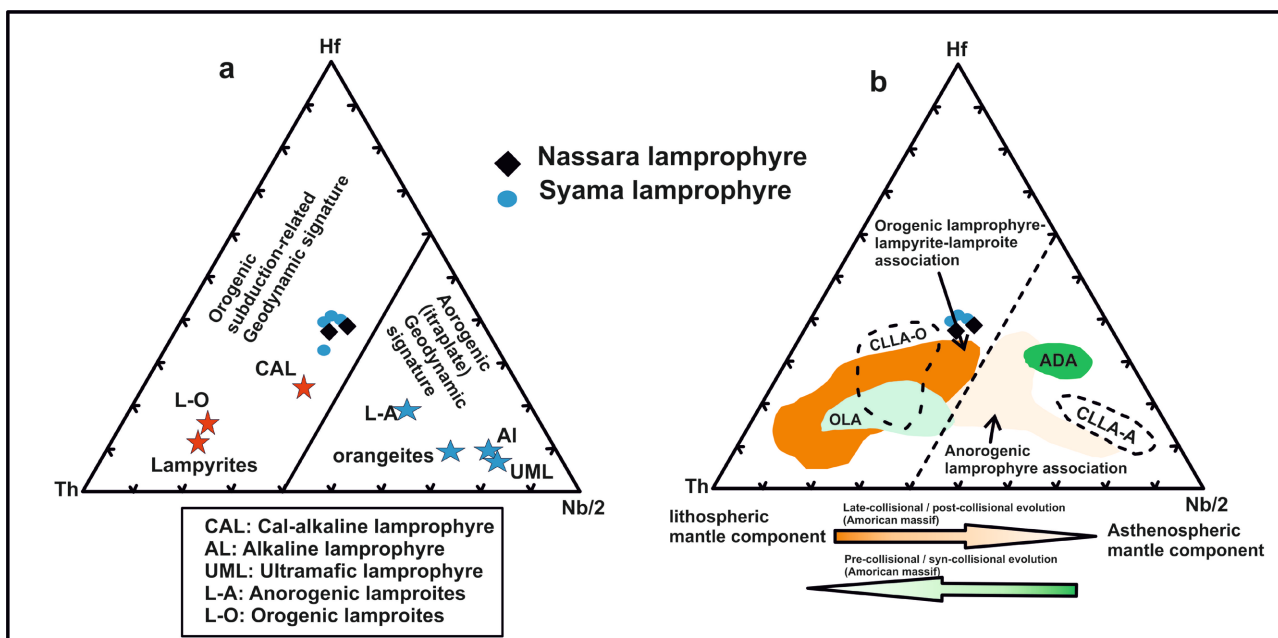


Figure 17. Diagram showing discrimination between orogenic and anorogenic contexts ([34]). (a) Positions of the Nassara and Syama lamprophyres in the Hf-Th-Nb/2 ternary diagram; (b) Post-collision orogenic subduction context for the Nassara and Syama lamprophyres in the same diagram.

8. Conclusions

At the Nassara mineralized zone, the host formations are cut by lamprophyre dykes. Petrographic and chemical data on the minerals and total rock show that these are lamprophyre of the spessartite type. These rocks are derived from depleted primitive mantle, enriched in LILE by fluids probably related to metasomatic activity.

The high Nb/Ta ratios in the Nassara lamprophyres are indicative of metaso-

matic activity, probably involving amphiboles and rutile in the mantle prior to melting.

The Nassara spessartite lamprophyres have a geodynamic signature marked by late to post-collisional orogenic subduction, as shown in the Th-Hf-Nb/2 ternary diagram in **Figure 17b**. They are late-orogenic to post-collisional, enriched in compatible elements (Cr, Ni, Co) and show a negative Ta-Nb-Ti (TNT) anomaly.

Lamprophyres are very often spatially and closely related to orogenic gold deposits, but are not the source of mineralization related to these deposits. Their presence in gold deposits is an indicator of crustal permeability, with a capacity to channel hydrothermal fluids at the time of emplacement. Mapping this type of rock in shear corridors could guide prospecting and help identify potential zones of hydrothermal fluid circulation.

Acknowledgements

At the conclusion of this article, the authors would like to thank the mining company B2Gold, through its chief geologist Mr. NARE Athanase, for allowing us to sample the various rocks for analysis. The WAXI-2 project funded the fieldwork and geochemical analyses. We would also like to thank the Institut de Recherche pour le Développement (IRD) for its logistical support.

Conflicts of Interest

The authors declare no conflicts of interest regarding the publication of this paper.

References

- [1] Le Maitre, R.W. (1989) A Classification of Igneous Rocks and Glossary of Terms (Recommendations of the International Union of Geological Sciences Sub-Commission on the Systematics of Igneous Rocks). Blackwell, Oxford, 193 p.
- [2] Rock, N.M.S. (1991) Lamprophyres. Blackie, Glasgow, 285 p.
<https://doi.org/10.1007/978-1-4757-0929-2>
- [3] Le Bas, M.J. and Streckeisen, A.L. (1991) The IUGS Systematics of Igneous Rocks. *Journal of the Geological Society*, **148**, 825-833.
<https://doi.org/10.1144/gsjgs.148.5.0825>
- [4] Leat, P.T., Thompson, R.N., Morrison, M.A., Hendry, G.L. and Dickin, A.P. (1988) Silicic Magmas Derived by Fractional Crystallization from Miocene Minette, Elkhead Mountains, Colorado. *Mineralogical Magazine*, **52**, 577-585.
<https://doi.org/10.1180/minmag.1988.052.368.03>
- [5] Wyman, D. and Kerrich, R. (1989) Archean Shoshonitic Lamprophyres Associated with Superior Province Gold Deposits: Distribution, Tectonic Setting, Noble Metal Abundances, and Significance for Gold Mineralization. *Economic Geology Monograph*, **6**, 651-667. <https://doi.org/10.5382/Mono.06.50>
- [6] Macdonald, R., Upton, B.G.J., Collerson, K.D., Hearn Jr., B.C. and James, D. (1992) Potassic Mafic Lavas of the Bearpaw Montana: Mineralogy, Chemistry, and Origin. *Journal of Petrology*, **33**, 305-346. <https://doi.org/10.1093/petrology/33.2.305>

- [7] Carlier, G., Lorand, J.P., Audebaud, E. and Kienast, J.R. (1997) Petrology of Unusual Orthopyroxene-Bearing Minette Suite from Southeastern Peru, Eastern Andean Cordillera: Al-Rich Lamproites Contaminated by Peraluminous Granites. *Journal of Volcanology and Geothermal Research*, **75**, 59-87.
[https://doi.org/10.1016/S0377-0273\(96\)00035-2](https://doi.org/10.1016/S0377-0273(96)00035-2)
- [8] Allibone, A.H., Campbell, M.T., Harrist, T., Etheridge, M., Munroe, S., Byrned, D., Amanor, J. and Gyapong, W. (2002) Structural Controls on Gold Mineralization at the Ashanti Gold Deposit, Obuasi, Ghana. In: Goldfarb, R.J. and Nielsen, R.L., Eds., *Integrated Methods for Discovery: Global Exploration in the Twenty-First Century*, Society of Economic Geology, Littleton, Special Publication 9, 65-93.
<https://doi.org/10.5382/SP.09.04>
- [9] Baratoux, L., Metelka, V., Naba, S., Jessell, M.W., Grégoire, M. and Ganne, J. (2011) Juvenile Paleoproterozoic Crust Evolution during the Eburnean Orogeny (~2.2-2.0 Ga), Western Burkina-Faso. *Precambrian Research*, **191**, 18-45.
<https://doi.org/10.1016/j.precamres.2011.08.010>
- [10] Ouedraogo, M.F. and Prost, A.E. (1986) Relationships between Schistosity and Folding within the Birimian Yako-Batie Greenstone Belt (Burkina Faso). *Comptes Rendus de l'Academie des Sciences*, **303**, 1713-1718.
- [11] Lombo, M., Caby, R. and Robineau, B. (1991) Etude structurale et géologique des séries birimienennes de la région de Kwademen, Burkina Faso, Afrique de l'Ouest. In: *Evolution et contrôle structural des minéralisations sulfureuses et aurifères pendant l'Eburnéen*, Université de Clermont Ferrand, Clermont-Ferrand, 1-192.
- [12] Metelka, V., Baratoux, L., Naba, S. and Jessell, M.W. (2011) A Geophysically Constrained Litho-Structural Analysis of the Eburnean Greenstone Belts and Associated Granitoid Domains, Burkina Faso, West Africa. *Precambrian Research*, **190**, 48-69.
<https://doi.org/10.1016/j.precamres.2011.08.002>
- [13] Ledru, P., Milési, J.P., Feybesse, J.L., Dommange, A., Johan, V., Diallo, M. and Vinchon, C. (1989) Tectonique transcurrente et évolution polycyclique dans le Birimien, Protérozoïque inférieur du Sénégal-Mali. *Comptes Rendus de l'Académie des Sciences Paris*, **308**, 117-122.
- [14] Milési, J.P., Ledru, P., Feybesse, J.-L., Dommange, A. and Marcoux, E. (1992) Early Proterozoic Ore Deposits and Tectonics of the Birimian Orogenic Belt, West Africa. *Precambrian Research*, **58**, 305-344. [https://doi.org/10.1016/0301-9268\(92\)90123-6](https://doi.org/10.1016/0301-9268(92)90123-6)
- [15] Feybesse, J.L., Billa, M., Guerrot, C., Duguey, E., Lescuyer, J.L., Milési, J.P. and Bouchot, V. (2006) The Paleoproterozoic Ghanaian Province: Geodynamic Model and Ore Controls, Including Regional Stress Modeling. *Precambrian Research*, **149**, 149-196. <https://doi.org/10.1016/j.precamres.2006.06.003>
- [16] Ouiya P., Siebenaller, L., Salvi, S., Béziat, D., Naba, S., Baratoux, L., Naré, A. and Franceschi, G. (2016) The Nassara Gold Prospect, Gaoua District, Southwestern Burkina Faso. *Ore Geology Reviews*, **78**, 623-630.
<https://doi.org/10.1016/j.oregeorev.2015.11.026>
- [17] Leterrier, J., Maury, R.C., Thonon, P., Girard, D. and Marchal, M. (1982) Clinopyroxene Composition as a Method of Identification of the Magmatic Affinities of Paleo-Volcanic Series. *Earth and Planetary Science Letters*, **59**, 139-154.
[https://doi.org/10.1016/0012-821X\(82\)90122-4](https://doi.org/10.1016/0012-821X(82)90122-4)
- [18] Béziat, D., Bourges, F., Débat, P., Lombo, M., Martin, F. and Tollon, F. (2000) A Paleoproterozoic Ultramafic-Mafic Assemblage and Associated Volcanic Activity in the West African Craton. *Precambrian Research*, **10**, 25-47.
[https://doi.org/10.1016/S0301-9268\(99\)00085-6](https://doi.org/10.1016/S0301-9268(99)00085-6)

- [19] Leake, B.E., et al (1997) Nomenclature of Amphiboles: Report of the Subcommittee on Amphiboles of the International Mineralogical Association, Commission on New Minerals and Mineral Names. *The Canadian Mineralogist*, **35**, 219-246.
- [20] Al'meev, R.R., Ariskin, A.A., Ozerov, A.Yu. and Kononkova, N.N. (2002) Problems of the Stoichiometry and Thermobarometry of Magmatic Amphiboles: An Example of Hornblende from the Andesites of Bezymyannyi Volcano, Eastern Kamchatka. *Geochemistry International*, **40**, 723-738.
- [21] Dick, H.J.B. and Bullen, T. (1984) Chromian Spinel as a Petrogenetic Indicator in Abyssal and Alpine-Type Peridotites, and Spatially Associated Lavas. *Contributions to Mineralogy and Petrology*, **86**, 54-76. <https://doi.org/10.1007/BF00373711>
- [22] Leblanc, M. (1985) Les Gisements de Spinelles Chromifères. *Bulletin de Minéralogie*, **108**, 587-602. <https://doi.org/10.3406/bulmi.1985.7876>
- [23] Irvine, T.N. (1967) Chromian Spinel as a Petrogenetic Indicator. Part 2. Petrographic Applications. *The Canadian Journal of Earth Sciences*, **4**, 71-103. <https://doi.org/10.1139/e67-004>
- [24] Peccerillo, A. and Taylor, S.R. (1976) Geochemistry of Eocene Calc-Alkaline Volcanic Rocks from the Kastamonu Area, Northern Turkey. *Contributions to Mineralogy and Petrology*, **58**, 63-81. <https://doi.org/10.1007/BF00384745>
- [25] Pearce, J.A. (1983) The Role of Sub-Continental Lithosphere in Magma Genesis at Destructive Plate Margins. In: Hawkesworth, C.J. and Norry, M.J., Eds., *Continental Basalts and Mantle Xenoliths*, Shiva, Nantwich, 230-249.
- [26] Rocks, N.M.S. (1987) The Nature and Origin of Lamprophyres: An Overview. Geological Society of London Special Publication 30, London, 191-226. <https://doi.org/10.1144/GSL.SP.1987.030.01.09>
- [27] Morin, D. (1998) La brèche intrusive de Rivard mise en place, nature et origine d'un lamprophyre ultrapotassique Grenvillien et de ses xénolites ultramafiques, région de Mont-Laurier, Québec. Doctoral Dissertation, Université du Québec, Institut national de la recherche scientifique, Québec.
- [28] Gill, R. (2010) Igneous Rocks and Processes: A Practical Guide. John Wiley & Sons, Hoboken.
- [29] Mitchell, R.H. (1994) Suggestions for Revisions to the Terminology of Kimberlites and Lamprophyres from a Genetic Viewpoint. In: Meyer, H.O.A. and Leonards, O.H., Eds., *Proceedings 5th International Kimberlite Conference 1. Kimberlites and Related Rocky and Mantle Xenoliths*, Companhia de Pesquisa de Recursos Mineiros, Brasilia, Spec. Publ. 1/A, 15-26.
- [30] Moayyed, M., Moazzen, M., Calagari, A.A., Jahangiri, A. and Modjarrad, M. (2008) Geochemistry and Petrogenesis of Lamprophyric Dykes and the Associated Rocks from Eslamy Peninsula, NW Iran: Implications for Deep-Mantle Metasomatism. *Chemie der Erde*, **68**, 141-154. <https://doi.org/10.1016/j.chemer.2006.04.002>
- [31] McDonough, W.F. and Sun, S. (1995) The Composition of the Earth. *Chemical Geology*, **120**, 223-253. [https://doi.org/10.1016/0009-2541\(94\)00140-4](https://doi.org/10.1016/0009-2541(94)00140-4)
- [32] Foley, S., Tiepolo, M. and Vannucci, R. (2002) Growth of Early Continental Crust Controlled by Melting of Amphibolite in Subduction Zones. *Nature*, **417**, 837-840. <https://doi.org/10.1038/nature00799>
- [33] Wyman, D.A., Ayer, J.A., Conceição, R.V. and Sage, R.P. (2006) Mantle Processes in an Archean Orogen: Evidence from 2.67 Ga Diamond-Bearing Lamprophyres and Xenoliths. *Lithos*, **89**, 300-328. <https://doi.org/10.1016/j.lithos.2005.12.005>
- [34] Krmíček, L., Magna, T., Pandey, A., Chalapathi Rao, N.V. and Kynický, J. (2021)

Lithium Isotopes in Kimberlites, Lamproites and Lamprophyres as Tracers of Source Components and Processes Related to Supercontinent Cycles. Geological Society, London, Special Publications, 513. <https://doi.org/10.1144/SP513-2021-60>

- [35] Traoré, Y.D., Siebenaller, L., Salvi, S., Béziat, D. and Bouaré, M.L. (2016) Progressive Gold Mineralization along the Syama Corridor, Southern Mali (West Africa). *Ore Geology Reviews*, **78**, 586-598. <https://doi.org/10.1016/j.oregeorev.2015.11.003>
- [36] Rock, N.M., Groves, D.I., Perring, C.S. and Golding, S.D. (1989) Gold, Lamprophyres, and Porphyries: What Does Their Association Mean. *Economic Geology Monograph*, **6**, 609-625. https://doi.org/10.5382/Mono_06.47
- [37] Kerrich, R. and Wyman, D.A. (1994) The Mesothermal Gold-Lamprophyre Association: Significance for an Accretionary Geodynamic Setting, Supercontinent Cycles, and Metallogenic Processes. *Mineralogy and Petrology*, **51**, 147-172. <https://doi.org/10.1007/BF01159725>
- [38] Mueller, W. and Donaldson, J.A. (1992) Development of Sedimentary Basins in the Archean Abitibi Belt, Canada: An Overview. *Canadian Journal of Earth Sciences*, **29**, 2249-2265. <https://doi.org/10.1139/e92-177>
- [39] Taylor, W.R., Rock, N.M., Groves, D.I., Perring, C.S. and Golding, S.D. (1994) Geochemistry of Archean Shoshonitic Lamprophyres from the Yilgarn Block, Western Australia: Au Abundance and Association with Gold Mineralization. *Applied Geochemistry*, **9**, 197-222. [https://doi.org/10.1016/0883-2927\(94\)90007-8](https://doi.org/10.1016/0883-2927(94)90007-8)
- [40] Dubé, B., Williamson, K., McNicoll, V., Malo, M., Skulski, T., Twomey, T. and Sanborn-Barrie, M. (2004) Timing of Gold Mineralization at Red Lake, Northwestern Ontario, Canada: New Constraints from U-Pb Geochronology at the Goldcorp High-Grade Zone, Red Lake Mine, and the Madsen Mine. *Economic Geology*, **99**, 1611-1641. <https://doi.org/10.2113/99.8.1611>
- [41] Wyman, D., Kerrich, R. and Sun, M. (1995) Noble Metal Abundances of Late Archean (2.7 Ga) Accretion-Related Shoshonitic Lamprophyres, Superior Province, Canada. *Geochimica et Cosmochimica Acta*, **59**, 47-57. [https://doi.org/10.1016/0016-7037\(94\)00373-T](https://doi.org/10.1016/0016-7037(94)00373-T)